Investigation of novel organometallic and physicochemical properties of [Sr (C$_{10}$H$_{20}$O$_5$)$_2$·Co (SCN)$_4$]: SCCTC single crystal for NLO application

S. Ramkumar[1] · P. Malliga[1]

Abstract

A novel inorganic polymers and organic spacers (IPOS) derivative strontium cobalt chloride bis 15-crown-5-ether tetra ammonium thiocyanate (SCCTC) single crystal synthesis via solution growth technique. Initially, the detailed crystallography information of cell parameters and data structure were carried out by single crystal X-ray diffraction studies, which reveal that the orthorhombic system acquires centrosymmetric space group of *Pnma*. As-grown crystal chemical bonding assignments, elemental compositions confirmed by using energy dispersive X-ray and vibrational spectroscopy. Additionally, H-bond present in the prepared sample identified by CHNS analysis. In this work, the cut-off wavelength was found at 353 nm with band gap (Tauc's plot) of 3.22 eV can be ascertained from the UV–Visible-NIR spectrum. The prominent crystal growth mechanism were examined by using scanning electron microscope, chemical etching study to correlate the surface texture and reverse growth rate etch pattern. For device fabrication, lattice dynamics, thermal and mechanical properties are necessary for testing the sample assessment by thermogravimetric, Vickers hardness and dielectric measurement. Using single beam Z-scan technique under 633 nm excitation were carried out experimentally non-linear susceptibility, absorption coefficient and refractive index. The above results suggest that grown crystals have good transmittance, moderate thermal, mechanical and large susceptibility values. So, these properties turn into be potential materials for making optical device applications.

Keywords Slow evaporation method · Single crystal XRD · Elemental analysis · Z-scan studies

1 Introduction

Recent research has concentrated on growing newer metal–organic single crystal of great importance for high-performance device manufacturing. The intense research activity based on second and third-order nonlinear optical (SONLO and TONLO) properties is a

---

✉ P. Malliga
calltomp@gmail.com

[1] Department of Physics, Sathyabama Institute of Science and Technology, Chennai, Tamil Nadu 600119, India

prime factor producing a wide range of optical applications (Divya et al. 2021a, 2021b, 2021c; Joseph Arul Pragasam et al. 2018; Malliga and Joseph Arul Pragasam 2013; Anushya et al. 2022; Alosious Gonsago et al. 2011; Malliga et al. 2013). Specifically, inorganic polymers and organic spacers (IPOS) complex considerable scientific interest enhance the NLO efficiency. Compared to organic and inorganic materials, a metal organic compound possesses stronger physicochemical stability, a high laser damage threshold and promising NLO response (Karuppasamy et al. 2016; Ravisankar et al. 2021a; Cliffe et al. 2019; Saravanan et al. 2018; Divya et al. 2019a; Malliga et al. 2011a, 2012). Keeping this viewpoint nowadays, investigations are being continued to synthesize novel organometallic materials, while selecting the appropriate IPOS materials is widely used for many applications, including optical bi-stable devices, frequency doubling, tripling conversion, optical switching, optoelectronics and optical communications (Malliga et al. 2011b, 2011c; Malliga and Joseph Arul Pragasam 2015; Alosious Gonsago et al. 2012; Divya et al. 2019b).

The chemical formula of a bimetallic thiocyanate complex is AB $(SCN)_4$, where A is alkali earth metals (Sr^{2+}, Ba^{2+}, Mn^{2+}), B is transition metal ions (Co^{2+}, Zn^{2+}, Fe^{2+}), ligands (ammonium thiocyanate, urea, thiourea and thiosemicarbazide) are a predominant contribution to increasing the NLO efficiency. Therefore, these materials are suitable for high-power frequency conversion applications. As per the above-mentioned formula, both divalent metals (AB) and ligands (SCN^-) are major backbone formations of the IPOS skeleton structure. In these complexes, thiocyanate (SCN^-) is a good chromophore combining the heteroatoms like nitrogen or sulphur. Based on the hard-soft-acid–base concept examined by Person and Balarew after attempts were made to design the multifunction coordination modes with thiocyanate, which build up a variety of molecular structures (Pearson 1963; Balarew and Duhlew 1984). In this category of material, crystal structure contains a unique charge transfer from metal to linkers or linkers to the metal complex, as proposed by Xu et al. (Xu et al. 1987). In the IPOS series structure, choosing host materials (crown ether), guests (metal complexes) and thiocyanate ligands form a wide variety of two-dimensional layered structures, depending upon the cavity diameter and coordination solids.

In this context, cobalt ion bonded to SCN^- of the sulphur site, strontium combined with 15-crown-5 ether, and formed the new crystalline arrangement of structure. A novel strontium cobalt chloride bis 15-crown-5-ether tetra ammonium thiocyanate (SCCTC) single crystal synthesis via solution growth technique. SCCTC is characterized by the structural study of single crystal XRD (SXRD), Fourier transform infrared (FTIR) spectroscopy, linear optical properties of UV–Vis-NIR, stability properties are thermal (TG/DTA) and Vickers micro-hardness, surface properties of chemical etching, high resolution (HR) scanning electron microscopy (SEM), elemental properties of energy dispersive spectroscopy (EDS), CHNS, electric properties of dielectric studies. Third order nonlinear optical (TONLO) properties determined by Z-scan studies under 633 nm, all the investigations are experimentally discussed.

2 Experimental procedure

2.1 Materials

All major raw materials were purchased AR-grade strontium chloride ($SrCl_2$) cobalt chloride ($CoCl_2$), 15-crown-5 ether ($C_{10}H_{20}O_5$) and ammonium thiocyanate (NH_4SCN).

2.1.1 Synthesis and growth

The growth process was carried out in de-ionized water, methanol and ethanol used for the chemical synthesis procedure:

$$SrCl_2 + CoCl_2 + 2(C_{10}H_{20}O_5) + 4[NH_4SCN] \rightarrow [Sr(C_{10}H_{20}O_5)_2 \cdot Co(SCN)_4] + 4NH_4Cl$$
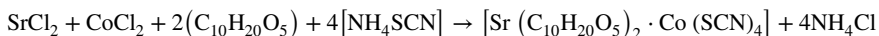
Initially, $SrCl_2$, $CoCl_2$ and NH_4SCN taken in a 1:1:4 ratio was dissolved in de-ionized water and stirred for one hour. After three addition, the mixture was stirred for 30 min to get a clear solution. An inorganic crown ether substance was added dropwise above mixture and then the solution was continuously stirred for 8 h. During this stage, a small precipitation settled down in the bottom of beaker. To avoid this, growth temperature was optimized to $+5$ °C near comfortable temperature. The prepared transparent solution was cautiously filtered into another beaker and sealed for crystallization and the system was kept free from external disturbances. The blue-colored seed crystal with dimensions of $11 \times 5 \times 2$ mm^3 could be harvested from 25 to 30 days. The photograph and chemical scheme of SCCTC as shown in Fig. 1.

2.1.2 Solubility measurement

Solubility of SCCTC intent on using assorted solvents like methanol, ethanol and de-ionized water measured at various temperatures (30 to 50 °C). Here, the observed solubility curve reveals, very less in de-ionized water quite better soluble in methanol and ethanol. Therefore, the title compound was grown by using mixed solvents in the ratio of 2:2:1. Figure 2, a typical solubility diagram reveals the possibility of growing SCCTC crystal by using slow evaporation method.
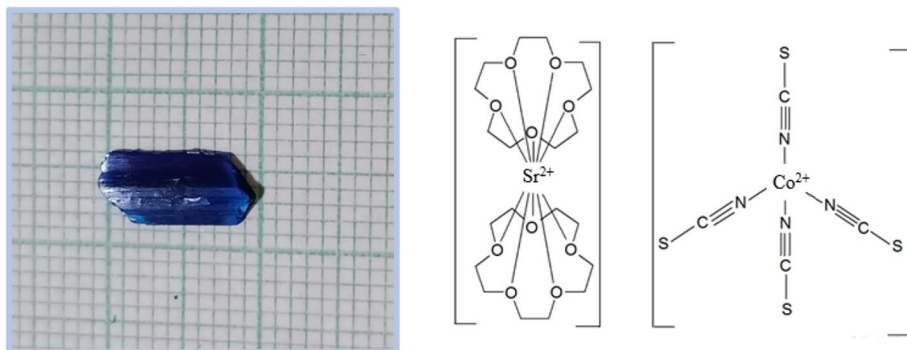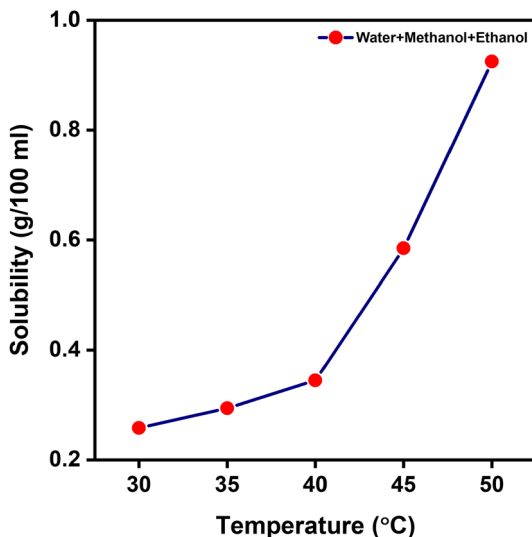

Fig. 1 Photograph and chemical scheme of SCCTC single-crystal

Fig. 2 Solubility curve of
SCCTC

3 Results and discussions

3.1 Crystallographic studies: single crystal X-ray diffraction

The SCCTC structure were investigated by a Bruker-Kappa APEX II CCD diffractometer and molybdenum Kα (0.7107 Å) radiation using ω/2θ scan mode. Cell refinement and data reduction can be accompanied by using the SAINT (Bruker APEX2 and SAINT, Bruker AXS 2008). A cumulative of 84,762 unique reflections were contained out of these 3629 individual reflections (I > 2σ (I)) and 214 variables of parameters. SADABS (Sheldrick 1996) was used to correct the intensities for Lorentz, polarization effects and absorption corrections. SCCTC structure was solved by a direct method for this process implemented as SHELXS97 (Sheldrick 2008), refined by using SHELXL 2018 (Ravisankar et al. 2021b) to include the position of all non-hydrogen (H). The reliability (R) factor was 0.08. SCCTC crystallizes orthorhombic structure and acquires centrosymmetric space group *Pnma* with lattice dimensions: $a = 16.085$ (3) Å, $b = 12.539$ (2) Å, $c = 17.984$ (3) Å, $\alpha = \beta = \gamma = 90°$ and volume (V) = 3627.42(11) Å^3. Table 1 summarizes the crystallographic refinement data of the grown SCCTC crystal. The structure was first time deposited in Cambridge Crystallographic Data Centre (CCDC No: 2258465) Fig. 3a is a 30% probability ellipsoid level ORTEP plot of the title molecule numbering pattern. In this structure, both Co^{II} ions and ammonium thiocyanate ligands are placed in the same plane whereas 15-crown-5-ether and Sr^{II} ions are located on the mirror plane, leading to a chain-like arrangement. Hence the ORTEP plot of the molecule shows a sandwich-like configuration. The molecular and crystal packing diagram of SCCTC is shown in Fig. 3b and c. Table 2 represented H-bond data.

Table 1 Crystal data, data collection and structure refinement

Identification code	SHELX
Chemical formula	$C_{24} H_{40} Co N_4 O_{10} S_4 Sr$
Formula weight	819.39
Crystal system, space-group	Orthorhombic, *Pnma*
Cell dimensions	$a = 16.085(3)\text{Å},$ $b = 12.539(2)\text{Å},$ $c = 17.984(3) \text{ Å}:$ $\alpha = \beta = \gamma = 90°$
T (K)	296(2)
λ (Å)	0.7107
V (Å^3)	3627.42(11)
D_x (g/cm^3)	1.500
Z	4
hkl ranges	$-19 <= h <= 19,$ $-15 <= k <= 15,$ $-21 <= l <= 21$
Θ range (º)	3.686–70.243
No. of parameters	214
Goodness of fit	1.059
R (F) [I > 2σ (I)]	0.0838
R (F) (all data)	0.0962
Max/min Δρ (e.Å^{-3})	0.7533 and 0.4660

3.2 Optical studies

For NLO studies, optical properties are very essential such as absorbance coefficient (α), transmittance and band gap (E_g) carried out by Shimadzu UV 3600 over a wide range from 200 to 2000 nm. Figure 4a and b show the grown crystal ultraviolet spectrum. As seen in the transmittance spectrum, the sample cut-off wavelength was found at 353 nm. The material has higher transmittance in the visible and near infrared regions, so we concluded the grown crystal is applicable for NLO device applications. The UV cut-off wavelength of SCCTC is far better than other thiocyanate family materials such as MFCTC (338 nm), NMTC (344 nm). Likewise, in both absorption and transmission spectra, a broad band was identified up to 1200 nm (IR region) due to the d-d transition presence of Co^{2+} ion incorporated in the SCCTC. The band gap (E_g) was measured by plotting Tauc's relation (Raghavan et al. 2010).

$$E_g = \frac{1240}{\lambda} eV \tag{1}$$

Here, E_g was drawn between $(\alpha h \gamma)^2$ and photon energy ($h\gamma$). The direct bandgap (DBG) value of the as-prepared sample was found to be 3.22 eV shown in Fig. 4c. The title compound (SCCTC) revealed better optical bandgap value compared with other organometallic materials like NMTC (3.1 eV), MFCTC (3.6 eV) (Ramish et al. 2013; Vijayabhaskaran and Ramachandra Raja 2013).
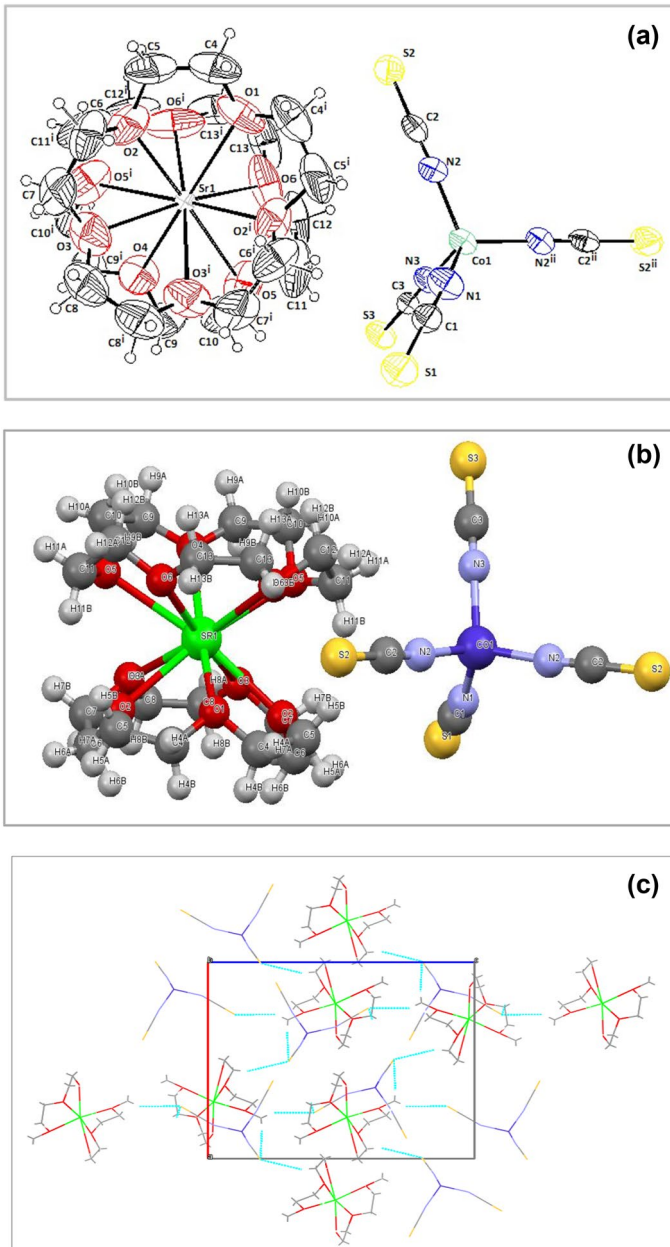
Fig. 3 a ORTEP plot of the molecule with atom numbering scheme drawn at 30% probability ellipsoid level. **b** Molecular structure of SCCTC. **c** The SCCTC crystal packing diagram, hydrogen bonds are shown as dashed lines

Table 2 Hydrogen bond data and angle (Å and °) of the compound

D-H…A	d (D-H)	d (H…A)	d (D…A)	<(DHA)
C11-H11B…O2^i^	0.97	2.58	3.28(3)	129
C13-H13B…S2 ^ii^	0.97	2.82	3.773(16)	168.1
C6-H6A…S1^iii^	0.97	2.98	3.779(18)	143.3
C8-H8A…S3^iv^	0.97	3.02	3.733(14)	131.4
C10-H10B…S2^v^	0.97	2.89	3.794(16)	154.8
C13-H13A…S1 ^vi^	0.97	2.93	3.654(14)	132.3

Symmetry operators: (i) x, − y+3/2, z (ii) x, − y+1/2, z (iii) x, y+1, z (iv) − x, − y+1, − z+1 (v) x − /2, y, − z+1/2 (vi) − x+1/2, − y+1, z − 1/2
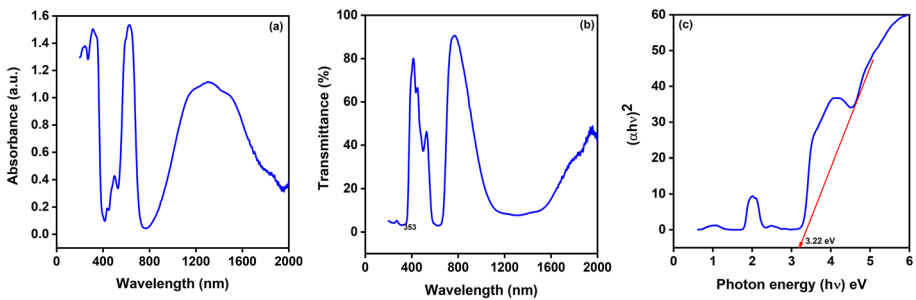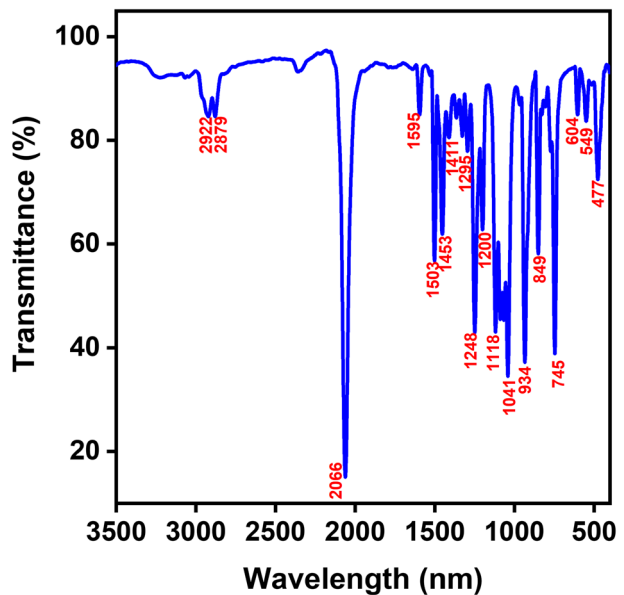

Fig. 4 UV–Vis-NIR **a** absorbance, **b** transmittance and **c** band gap spectrum of SCCTC

Fig. 5 FT-IR spectrum of SCCTC

Table 3 FT-IR functional group assignments of SCCTC

FT-IR Wave Number (cm^{-1})	Band assignments
2922 and 2879	C-H stretching vibrations
2066	CN stretching vibration of thiocyanate group
1503	CH$_2$ deformation of 15-crown-5 ether
1453	CN stretching vibration mode coordinated with Co atoms
1295, 1248 and 2922	CH$_2$ bending vibrations
849 and 934	Twice CS stretching vibration modes
549	Metal-Nitrogen stretch
477	Bending vibrations of SCN$^-$
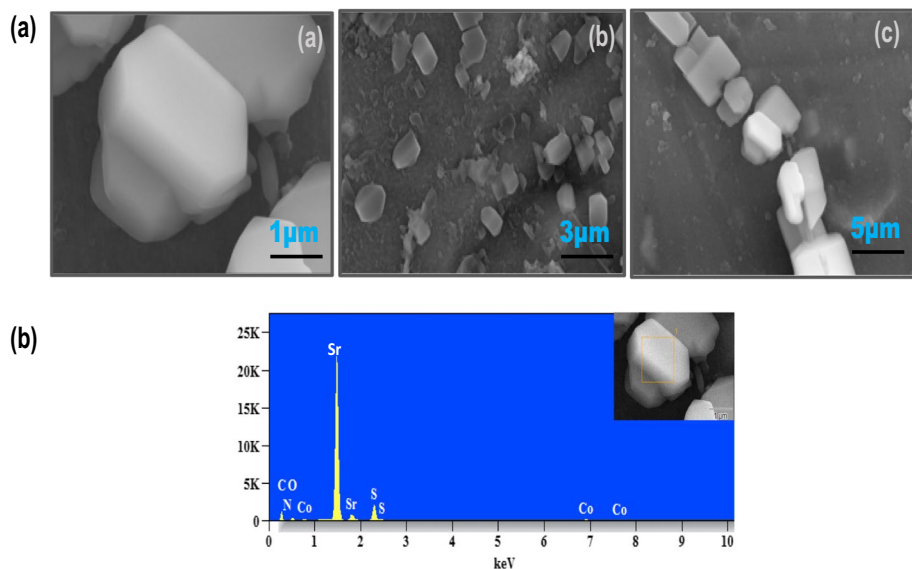
Fig. 6 **a** HR-SEM Micrograph images for SCCTC single-crystal at various magnifications. **b** EDS Spectrum for SCCTC

3.3 FT-IR spectroscopy

The prepared sample chemical bond information were observed by a Bruker IFS66V operating in ATR mode (400–4000 cm^{-1}). The existence of functional groups was displayed in Fig. 5. The peaks 2922 and 2879 cm^{-1} represent C-H stretching vibrations. A strong absorption peak of CN stretching vibration of thiocyanate group SCN$^-$ observed at 2066 cm^{-1} (Ravisankar et al. 2022). The bending vibrations of SCN$^-$ and twice CS stretching vibration modes were observed at 477, 849 and 934 cm^{-1}, respectively. The mid-frequency region of 1503 cm^{-1} is allotted to the CH$_2$ deformation of 15-crown-5 ether. A peak occurring at 1453 cm^{-1} was observed and referred to as CN stretching vibration mode coordinated with Co atoms. Due to the observed CH$_2$ bending, three low-intensity peaks were discovered at 1295, 1248 and 2922 cm^{-1} (Cynthia and Suresh

Table 4 EDS data of SCCTC

Elements	Mass (%)	Atom (%)
C	32.447	49.866
S	13.645	7.856
N	10.419	13.731
O	19.869	22.921
Co	6.335	1.984
Sr	17.287	3.642
Total		100

Table 5 Elemental composition of SCCTC crystal

Element	N (%)	C (%)	H (%)	S (%)
Experimental	7.407	34.602	5.003	15.089
Calculated	6.84	35.18	4.92	15.65

sagadevan et al. 2017). The metal-nitrogen stretching falls at 549 cm^{-1}. The SCCTC functional group assignments are listed in Table 3.

3.4 HR-SEM and EDS mapping

SCCTC-grown crystals were examined by the HITACHI S4800 instrument images and were taken with an effective voltage of 10 kV in a high vacuum. The as-prepared sample structural micrograph is displayed in Fig. 6a. Usually, crystal growth mechanisms were done by the slow evaporation method, during the growth period different layers are formed above the surface captured at 1, 3 and 5 μm. Additionally, an estimation of elements proportions at a different position is exactly identified by EDS analysis. Figure 6b reveals that strontium (Sr), Cobalt (Co), chlorine (CL) and thiocyanate ligand (SCN$^-$) are presented in the EDS mapping. Thus, observed experimental data and theoretical values are in fairly good agreement, as given in Table 4.

3.5 Elemental analysis

CHNS analysis is employed to determine the existence of as-prepared compounds (C_{24} H_{40} Sr Co N_4 O_{10} S_4). The elemental weight percentage data were obtained experimentally using a Vario EL cube analyzer. The observed C, H, N and S values are listed in Table 5. Thus, the SCCTC calculated chemical composition nearly matched the experimental values. Hence the title compound elements correlated along with FTIR and SXRD.

3.6 Chemical etching studies

For device fabrication defect fewer crystals are needed, hence growing a good quality single crystal mainly depends on using desirable solvents. The growth process information is based on structural features and reverses growth rate employed by Olympus high-resolution optical microscope. The SCCTC crystal surface layer was soaked with mixed etching
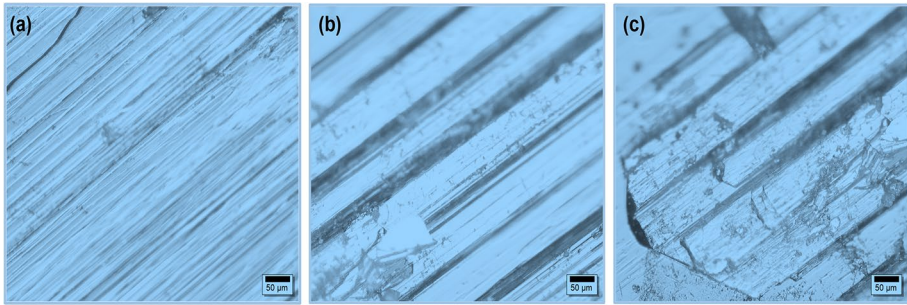
Fig. 7 **a** without etching surface, **b** etching 10 s, and **c** After etching 15 s for SCCTC single-crystal

agents such as ethanol, methanol and de-ionized water (2:2:1) during the etching period from 5 to 15 s. Figure 7a, without etching the SCCTC surface. The layered etch pattern was observed after 10 s of the etching period as shown in Fig. 7b. After 15 s etching time there was no obvious variations in the shape (Fig. 7c). Etch pit density (EPD) ratio is given by

$$\text{Etch pit density} = (\text{Number of etch pattern})/(\text{Area}) \qquad (2)$$

An estimated value of EPD is 2×10^6 cm^{-2}, which reveals the formation of step-growth nucleation (layer by layer) etch pit pattern that indicates a 2D growth mechanism.

3.7 Mechanical studies

Vickers method for assessing the grown crystal solid state property plays a vital role in device fabrication. Mechanical strength was carried out by an econometric VH-1MD hardness tester with diverse loads varying from 10 to 100 g. The static force was applied slowly on the SCCTC sample surface causing, dislocation in the indentation region. On higher
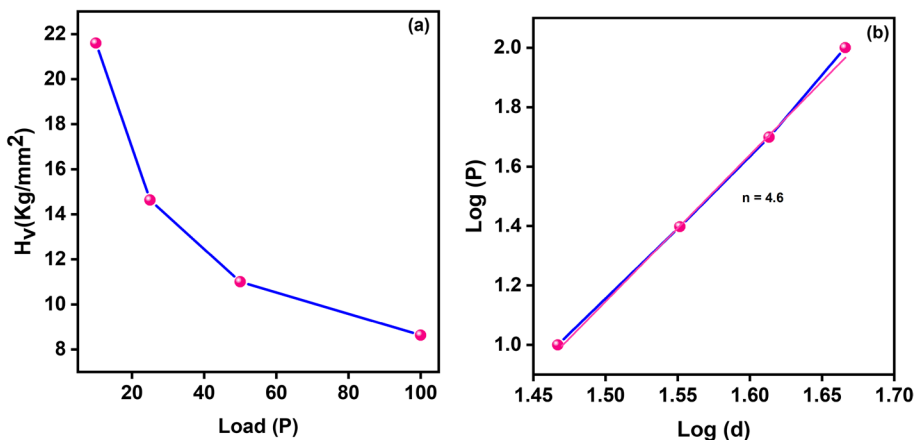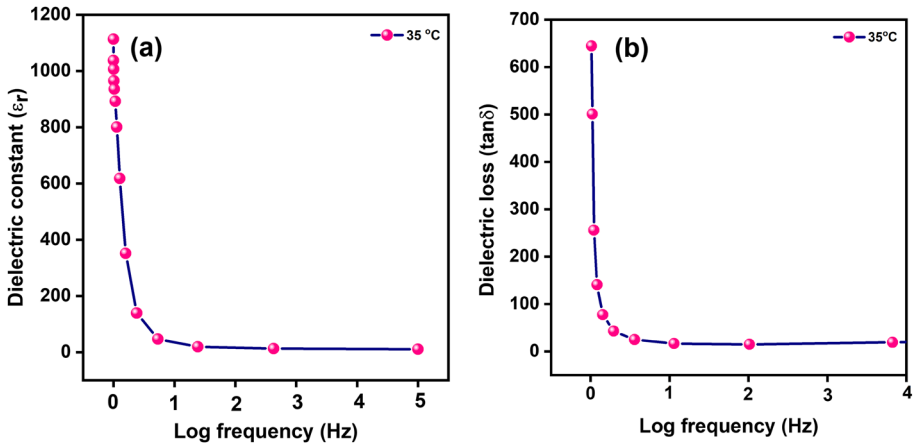

Fig. 8 **a** Vickers hardness Vs Load (P), **b** Log (P) Vs Log (d)

Table 6 Vickers hardness values of SCCTC single-crystal

S. No	Load (P) g	Vickers Hardness(Hv) Kg/mm^3
1	10	21.59
2	25	14.62
3	50	10.99
4	100	8.62

Fig. 9 **a** Dielectric constant (ε') Vs Log frequency (Hz) **b** Dielectric loss (tan δ) of SCCTC Vs Log frequency (Hz)

loadings beyond 100 g, cracks appear on the surface. For each load, the indentation length (d) was noted. Estimated hardness relation (Onitsch 1947)

$$H_v = 1.854 \frac{P}{d^2} \left(\frac{\text{Kg}}{\text{mm}^2} \right) \tag{3}$$

Figure 8a shows Hv variation with load P. It is noted that the hardness number is decreasing with increasing load. Using the straight-line slop method, Fig. 8b is drawn between log (P) with log (d) employing a scheme of least square fit. As reported by Onitsch, the work-hardening coefficient (n) value is 4.6. Accordingly, SCCTC corresponds to a soft category material matched with other available organometallic thiocyanate crystals such as BCMTC (3) and TTPC (2.9) (Ravisankar et al. 2021c; Sakthi et al. 2016). The title compound Hv values are shown in Table 6.

3.8 Dielectric studies

The electrical conduction of solids is widely used in electro-optical device applications. At room temperature, dielectric properties and polarization mechanisms were investigated using a Hioki 3532–50 LCR meter with a frequency range of 1 Hz to 5 MHz. The dielectric constant (ε_r) dielectric loss (tan δ) can be expressed as (Miller 1964):

$$\varepsilon_r = \frac{Cpd}{\varepsilon_0 A} \tag{4}$$

$$\tan\delta = \varepsilon''/\varepsilon' \tag{5}$$

where, C and d signify the capacitance (Farads), thickness (mm), A and ε_o specify permittivity (8.854×10^{-12} F/m), area of cross-section (cm). Figure 9a plotted for ε_r against log frequency. Generally, solid materials are powerfully dependent on divisions of polarization (electronic, ionic, orientation and space charge) (Asokan and Kalainathan 2017). It was observed at lower frequencies, the ε_r becomes higher and this may be attributed to the existence of space charge polarization. It is noticed that most of the polarization is active at higher frequencies except for electronic polarization. Figure 9b displays log frequency against dielectric loss at room temperature. It implies that the power dissipation is proportional to the dielectric loss and promotes good crystalline nature of samples with lesser defects, as well as SEM and etching studies.

3.9 Estimation of dielectric solid state parameters (SSP)

SSP are important for exploring numerous functions for instance plasma energy ($\hbar\omega_p$), Penn gap (E_P), Fermi energy (E_F) and electronic polarizability (α) were calculated using the value of a dielectric constant. As norms of typical procedure, theoretical calculation always depends on the number of valence electrons obtainable in a given structure.

Density (ρ) is given by Ravisankar et al. (2022)

$$\rho = \frac{MZ}{N \cdot V} \tag{6}$$

M = 819.39 g/mol. molecular weight ($C_{10}H_{20}O_5$) unit cell (Z = 4), 6.023×10^{23}, Avogadro's number (N_A) and cell volume (V) 3627.42(11) $\mathring{A}^3$. An estimated density (ρ) value confirmed with 1.50 g/cm^3.

Plasma energy ($\hbar\omega_p$) given by Jackson (1978)

$$\hbar\omega_P = 28.8 \left(\frac{Z' \times \rho}{M} \right)^{\frac{1}{2}} \tag{7}$$

Cumulative number of valence electrons Z' = [(24×Z'$_C$) + (44×Z'$_H$) + (1×Z'$_{Co}$) + (1 ×Z'$_{Sr}$) + (4×Z'$_N$) + (10×Z'$_O$) + (3×Z'$_S$) = 267. The values of corresponding elemental valence are C (4), H (1), Co (9), Sr (2), N (5), O (6) and S (6), for substitutions. Here ε_r is 1 MHz. The relationship between Penn model, E_P and E_F given by Penn (1962); Ravindra and Srivastava 1980)

$$E_p = \frac{\hbar\omega_P}{(\varepsilon' - 1)^{\frac{1}{2}}} \tag{8}$$

$$E_F = 0.2948 \left(\hbar\omega_P \right)^{\frac{4}{3}} \tag{9}$$

Additionally, we calibrated electronic polarizability (α) using the relations

$$\alpha = \left[\frac{(\hbar\omega_P)^2 S_0}{(\hbar\omega_P)^2 S_0 + 3E_p^2}\right] \times \frac{M}{\rho} \times 0.396 \times 10^{-24} \text{ cm}^3 \tag{10}$$

$$S_0 = 1 - \left[\frac{E_p}{4E_F}\right] + \frac{1}{3}\left[\frac{E_p}{4E_F}\right]^2 \tag{11}$$

where S_o is constant, then the electronic polarizability (α) of the SCCTC is used to define the Clausius Mossotti (CM) relation, band gap (E_g) and coupled dipole method (CDM) (Nijboer and Renne 1968).

$$\alpha = \frac{3M}{4\pi N_A \rho}\left(\frac{\varepsilon' - 1}{\varepsilon' + 2}\right) \tag{12}$$

$$\alpha = \left[1 - \frac{\sqrt{Eg}}{4.06}\right]\left[\frac{M}{\rho}\right]0.396 \times 10^{-24} \text{ cm}^3 \tag{13}$$

$$\alpha = \frac{Z' e^2}{m_Q \omega_0^2} \tag{14}$$

where Z' cumulative number of valence electrons, 1.602×10^{-19} electron charge, 9.1×10^{-28} mass of the electron and 'ω_o' natural frequency ($2\pi f_o$), here 'f_o' is 1 MHz. The above results reveal electronic polarizability is considered as the most important factor at room temperature which is carefully calculated and noted in Table 7.

3.10 Thermal Studies

TG–DTA has carried out a NETZSCH STA 449F3 analyzer measured under nitrogen atmosphere ranging from 20 to 900 °C, at heat capacity rate of 10 °C. Thermal stability and decomposition temperatures are displayed in Fig. 10. The TG curve confirms that grown SCCTC is stable up to 207 °C, below this temperature no phase changes didn't happen in the stage. The above mentioned stability material has good crystalline behavior. DTA curve shows three endo-thermic peaks at 226, 382 and 398 °C, respectively. However,

Table 7 Solid-State parameter of SCCTC single-crystal

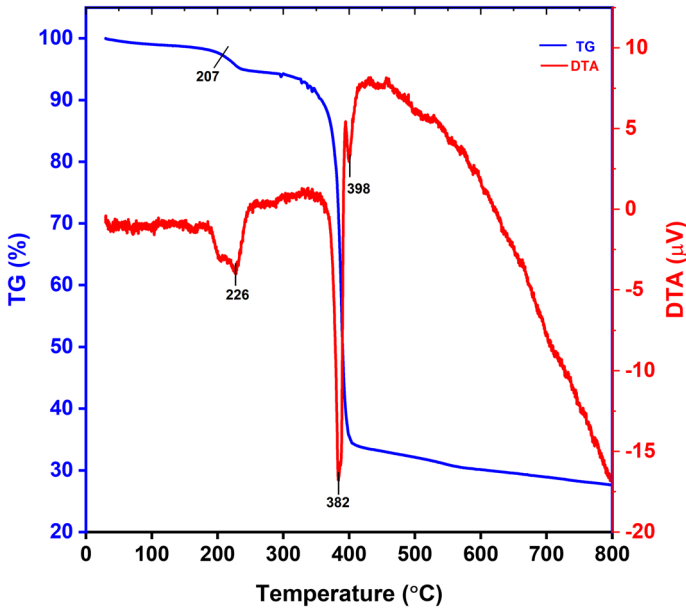| SSP-factors	Calculated values of SCCTC crystal
Plasma energy ($\hbar\omega_p$) eV	20.133
Penn gap energy (E_P) eV	0.8105
Fermi energy (E_F) eV	15.985
Electronic polarizability (α) using Penn analysis (cm³)	2.152×10^{-22}
Electronic polarizability (α) with CM relation (cm³)	2.155×10^{-22}
Electronic polarizability (α) with E_g (cm³)	1.207×10^{-22}
Electronic polarizability (α) with CDM (cm³)	7.629×10^{-22}

Fig. 10 TG–DTA trace of SCCTC

the first stage of decomposition occurs at 226 °C due to the presence of 15-Crown-5, Co (NH₄SCN) in the SCCTC sample. The second decomposition (382 °C) may be due to the release of metal sulfides, nitrogen gas and cyanogen. Third weight loss occurs at 398 °C, which agrees with the decomposition of the sample. We concluded that the material stability was obviously confirmed at 207 °C, which shows good crystalline behavior of the prepared sample. Furthermore, SCCTC has far better stabilization comparable to well-known bimetallic thiocyanate complex crystals like AMCTC (151.7 °C) and MCCTC (171 °C) (Rajarajan and K. Sendil Kumar 2013; Ramesh et al. 2020).

3.11 Z-scan: third-order non-linear optical studies

In the present study, the Z-scan technique were used to find the prime factors such as non-linear optical absorption coefficient (n_2), refractive index (β) and third-order susceptibility (χ^3) assessed by open (OA) and closed aperture (CA) patterns. He–Ne laser to generate a Gaussian laser beam source operated at 633 nm to focus the focal length ($f = 10$ cm) of the sample position. For the open type, a lens is placed before the detector whereas in closed aperture replaces lens to transmit a laser beam propagated through the sample. Figure 11a shows that OA measurements exhibit enhanced transmittance at the focus due to reverse saturable absorption (RSA) at high intensity. Figure 11b depicts the CA pattern, which reveals a transmittance valley to the peak indicating that the sample exhibits a positive nonlinearity due to a self-focusing (SF) effect. Rayleigh range (Z_R) calculated value is 0.76 mm, under the condition $Z_R < < L$ (Shettigar et al. 2007). ΔT_{v-p} is the transmittance difference (valley-peak), linear aperture transmittance (S) value is 0.52 and axis phase shift ($\Delta\Phi$) is found to be 0.24.

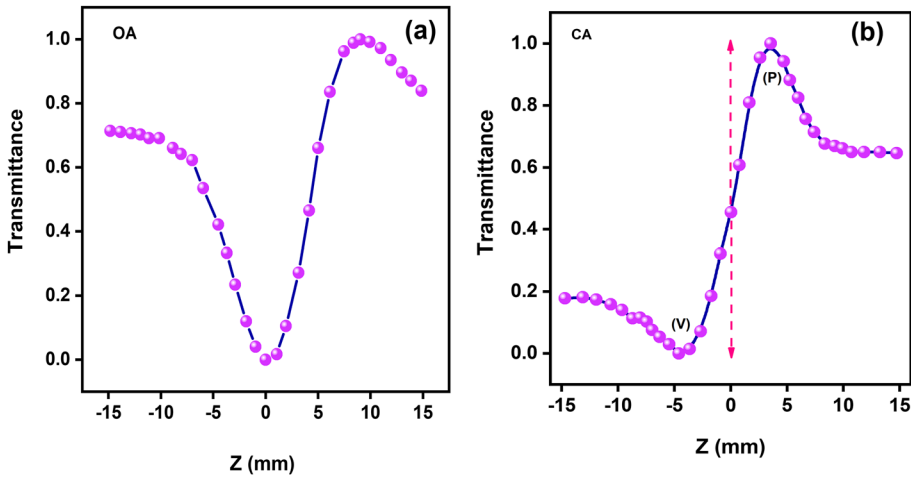Refractive index (n_2) and absorption (β) relations are given by Sheik-Bahae (1990)

Fig. 11 **a** Open, **b** Closed aperture Z-scan patterns of SCCTC single-crystal

$$n_2 = \frac{\Delta\Phi}{KI_oL_{eff}}\left(\frac{m^2}{w}\right) \tag{15}$$

$$\beta = \frac{2\sqrt{2}\Delta T}{I_oL_{eff}}\left(\frac{m}{w}\right) \tag{16}$$

Here, 'K' wave vector ($2\pi/\lambda$), the intensity of laser beam (I_o), ΔT transmittance value of open aperture and L_{eff} is effective sample thickness.

Real and Imaginary χ^3 relations given by Desalvo et al. (1993)

$$R_e\left(\chi^3\right)esu = \frac{10^{-4}\varepsilon_o C^2 n_o^2 n_2}{\pi}\left(\frac{cm^2}{w}\right) \tag{17}$$

$$I_m\left(\chi^3\right)esu = \frac{10^{-2}\varepsilon_o C^2 n_o^2 \lambda\beta}{4\pi^2}\left(\frac{cm}{w}\right) \tag{18}$$

where, $\varepsilon_0 = 8.854\times10^{-12}$ F/m is permittivity, 3×10^8 m/s velocity of light in vacuum (C) and 'n$_o$' refractive index liner term.

The real part added to imaginary parts of $\chi.^3$ relations (Stryland et al. 1998)

$$\chi^3 = \sqrt{\left(R_e\left(\chi^3\right)\right)^2 + \left(I_m\left(\chi^3\right)\right)^2} \tag{19}$$

The second-order hyper polarizability (γ) and correction factor (f) (Subashini et al. 2011).

$$\gamma = \frac{\chi^{(3)}}{N^* f^4} \tag{20}$$

$$f = \frac{(n_0^2 + 2)}{3} \qquad (21)$$

The estimated third-order NLO values $n_2 = 3.885 \times 10^{-9}$ cm^{2}W^{-1} and $\beta = 0.317 \times 10^{-5}$cmW^{-1}, respectively. Therefore, the calculated χ^3 value is 1.84×10^{-5}esu also the second-order hyper polarizability (γ) value is 4.36×10^{-27}esu. The above results reveal the title compound used for frequency tripling and optical switching applications (Priyadharshini et al. 2023; Shenbagarajan et al. 2023; Manimekalai et al. 2023; Jayaprakash et al. 2023; Shanthi et al. 2023; Johnson et al. 2018, 2019a, 2019b). The organometallic thiocyanate family CMTC (Hegde et al. 2018) crystal compared to SCCTC have a greater value of χ^3 summarized in Table 8.

4 Conclusion

The reported single-crystal SCCTC was grown by the slow evaporation method. SXRD studies reveal an orthorhombic structure with a space group of *Pnma*. Through FT-IR spectroscopy, the existence of metal-nitrogen vibrations (549 cm^{-1}) and CN stretching molecular vibrations (2066 cm^{-1}) of grown crystal functional groups was verified. The sample cut-off wavelength was found at 353 nm with an optical bandgap value of 3.22 eV. Additionally, in the case of reverse growth rate, surface morphology was examined by using etching and HR-SEM analysis. These findings led us to the conclusion shows that the

Table 8 Z-scan measurement details and the various parameters of the SCCTC single-crystal compared to CMTC

Z-scan parameters	SCCTC	CMTC
Laser type	He–Ne laser	Nd:YAG laser
Wavelength of laser (nm)	633	532
Focal length (f) cm	20	–
Laser beam-diameter (cm)	0.1	–
Sample thickness (cm)	0.1	–
Aperture radius (mm)	3.3	–
Intensity of the laser (KW/cm^2)	25	–
Optical path distance (mm)	1	–
Beam waist (ω_o) μm	12.04	–
Rayleigh length (Z_R) mm	0.76	–
Effective thickness (L_{eff}) mm	0.256	
Refractive index n_2 (cm^2/W)	3.885×10^{-9}	8.89×10^{-8}
Absorption coefficient β (cm/W)	0.317×10^{-5}	2.1×10^{-6}
Real part of TONLO [R_e (χ^3)] (cm^2/W)	13.070×10^{-6}	14.27×10^{-6}
Imaginary part of TONLO [I_m (χ^3)] (cm/W)	5.386×10^{-6}	0.13×10^{-6}
TONLO (χ^3) esu	1.84×10^{-5}	1.42×10^{-5}
Second order molecular hyper polarizability (γ) esu	4.36×10^{-27}	–
Number of molecules per cm^3 (N*)	$11.02 \times 10^{+20}$	–
Coupling factor (ρ*)	2.426	–

title compound has a good crystalline nature. The sample thermal stability was observed at 207 °C in the TG–DTA curve. The hardness testing reveals the material type is soft (n = 4.6) category. The grown single-crystal is superior to other organometallic crystals (AMCTC, MCCTC), according to thermal and hardness studies. The range of solid-state parameters such as Plasma (20.133 eV), Penn gap (0.8105 eV) and Fermi energy (15.985 eV) were theoretically calculated. The z-scan study performed under He–Ne laser excitation reveals RSA and SF nonlinearity. Higher NLO coefficients in the grown crystal can be a potential entrant for the RSA-based generation of short-pulse lasers. It is noteworthy that the title compound has excellent NLO properties that are used in optical switching applications.

Author Contributions SR contributed to the study conception and design. Material preparation, data collection and analysis were performed by SR and PM. The manuscript was written through contributions of all authors. All authors given approval to the final version of the manuscript.

Data Availability Not applicable.

Declarations

Conflict of interest The authors declare that they have no conflict of interest.

Ethical approval Not applicable.

References

Alosious Gonsago, C., Albert, H.M., Malliga, P., Joseph Arul Pragasam, A.: Growth and characterization of pure and thiourea doped L-histidine single crystals. Mater. Manuf. Processes **27**(3), 355–359 (2012). https://doi.org/10.1080/10426914.2011.58549

Alosious-Gonsago, C., Albert, H.M., Malliga, P., Joseph-Arul-Pragasam, A.: Crystallization, spectral, and thermal characterization of l-histidine methyl ester dihydrochloride (LHMED). J. Thermal Anal. Calorim. **107**(3), 1231–1235 (2011). https://doi.org/10.1007/s10973-011-1719-y

Anushya, G.B., Divya, M., Malliga, P.: χ3 measurement and second harmonic generation of organic–inorganic hybrid compounds headed for optoelectronic applications-L cysteine hydrogen orthoborate. Mater. Today Proc. **66**, 2198–2206 (2022). https://doi.org/10.1016/j.matpr.2022.06.037

Asokan, P., Kalainathan, S.: Bulk crystal growth, optical, electrical, thermal, and third order NLO properties of 2-[4-(Diethylamino)benzylidene]malononitrile (DEBM) single crystal. J. Phys. Chem. C **121**(40), 22384–22395 (2017)

Balarew, C., Duhlew, R.: Application of the hard and soft acids and bases concept to explain ligand coordination in double structures. J. Solid State Chem. **551**, 1–6 (1984)

Bruker APEX2 and SAINT, Bruker AXS Inc., Madison, Wisconsin, USA, (2008).

Cliffe, M.J., Keyzer, E.N., Dunstan, M.T., Ahmad, S., Devolder, M.F.L., Deschler, F., Morris, A.J., Grey, C.P.: Strongly colored thiocyanate frameworks with perovskite-analogue structures. Chem. Sci. **10**(3), 793–801 (2019)

Cynthia, S., Sagadevan, S., Mariappan, L.: Investigation on the linear, non-linear and optical studies an efficient organobimetallic zinc cadmium thiocynate nonlinear optical complex crystal. J. Mater. Sci Mater Electron **28**, 14787–14797 (2017)

Desalvo, R., Sheik-Bahae, M., Said, A., Hagan, D.J., Van Stryland, E.W.: Z-scan measurements of the anisotropy of nonlinear refraction and absorption in crystals. Opt. Lett. **18**, 194–196 (1993)

Divya, M., Malliga, P., Sagayaraj, P., Joseph-Arul-Pragasam, A.: Optical based electrical properties of thiourea borate NLO crystal for electro-optic Q switches. J. Electron. Mater. **48**, 5632–5639 (2019b). https://doi.org/10.1007/s11664-019-07377-2

Divya, M., Malliga, P., Joseph-Arul-Pragasam, A.: An investigation of opto-thermo-mechanical behavior of a borate family NLO crystal for photonic application. Brazilian J. Phys. **51**, 1625–1635 (2021a)

Divya, M., Anushya, G.B., Joseph-Arul-Pragasam, A., Vinitha, G., Malliga, P.: Third order measurements, thermal and mechanical stress tolerance studies of a nonlinear borate family hybrid crystal towards optoelectronic applications. Mater. Today: Proc. 1504–1510 (2021b). https://doi.org/10.1016/j.matpr.2021.07.246

Divya, M., Malliga, P., Divya, R., Vinitha, G., Joseph-Arul-Pragasam, A.: Studies on third order nonlinear optical properties of Nickel Boro Phthalate NLO crystal. Mater. Res. Express. **6**(11), 1–12 (2019a). https://doi.org/10.1088/2053-1591/ab4d6d

Divya, M., Malliga, P., Sagayaraj, P., Joseph-Arul-Pragasam, A.: Analysis on dielectric, thermal, and mechanical characteristics of nickel boro phthalate NLO crystal for optoelectronic applications. Crystal Res. Technol. **56**(9), 1–7 (2021c). https://doi.org/10.1002/crat.202000247

Hegde, T.A., Dutta, A., Vinitha, G.: χ^3 measurement and optical limiting behavior of novel semi-organic cadmium mercury thiocynate crystal by Z-scan technique: CMTC. Appl. Phy. A **124**, 1–10 (2018)

Jackson, J.D.: Classical Electro Dynamics, 3rd Edn. Wiley Eastern Limited, vol 819 (1978)

Jayaprakash, P., Raju, E., Hegde, T.A., Vinitha, G.: A self-defocusing third-order nonlinear optical material l-Alanine Barium Chloride single crystal used in optoelectronic device applications. Opt. Mater. **136**, 113406 (2023)

Johnson, J., Srineevasan, R., Sivavishnu, D.: Process development and characterization of centrosymmetric semiorganic nonlinear optical crystal: 4-dimethylaminopyridine potassium chloride. Physica B: Phys. Condensed Matter **S0921–4526**(18), 30239–30244 (2018). https://doi.org/10.1016/j.physb.2018.03.038

Johnson, J., Srineevasan, R., Siva-Vishnu, D., Allen-Moses, S.E.: Materials synthesis, band gap energy, yield strength and frequency doubling properties of 4-Dimethylaminopyridine lithium chloride: a semiorganic nonlinear optical crystal. Mater. Sci. Energy Technol. **2**, 543–550 (2019a)

Johnson, J., Srineevasan, R., Sivavishnu, D.: In depth study on growth aspects andcharacteristic properties of semiorganic nonlinear optical crystal: 4-dimethylaminopyridine copper chloride. Mater. Sci. Energy Technol. **2**, 226–233 (2019b). https://doi.org/10.1016/j.mset.2019.02.001

Joseph Arul Pragasam, A., Divya, M., Pani Vignesh, A., Vinitha, G., Malliga, P.: Analysis on linear and nonlinear optical properties of an efficient semi-organic crystal: thiourea borate. Opt. Laser Tech **107**, 428–434 (2018). https://doi.org/10.1016/j.optlastec.2018.06.003

Karuppasamy, P., Sivasubramani, V., Senthil-Pandian, M., Ramasamy, P.: Growth and characterization of semi-organic third order nonlinear optical (NLO) potassium 3, 5- dinitrobenzoate (KDNB) single crystals. RSC Adv. **6**, 109105–109123 (2016)

Malliga, P., Joseph-Arul-Pragasam, A.: Growth and characterization of pure and thiourea-doped l-alanine single crystals for NLO devices. J. Russ. Laser Res. **34**(4), 346–350 (2013)

Malliga, P., Alosious-Gonsago, C., Sagayaraj, P., Joseph-Arul-Pragasam, A.: Crystal growth, spectral, optical, and thermal characterization of glycyl-l-alanine hydrochloride (GLAH) single crystal. J. Therm. Anal. Calorim. **110**(2), 873–878 (2011c). https://doi.org/10.1007/s10973-011-1955-1

Malliga, P., Joseph-Arul-Pragasam, A.: Crystal growth, thermal, and optical studies: thiourea Glycyl-L-alanine single crystals. Chin. J. Phys. **53**, 111–124 (2015)

Malliga, P., Alosious Gonsago, C., Joseph-Arul-Pragasam, A.: Effect of thiourea doping on a novel amino acid crystal: GLAHCl. IntJ. Appl. Bioeng. **5**(2), 1–5 (2011a).

Malliga, P., Alosious-Gonsago, C., Joseph-Arul-Pragasam, A.: Structural and optical studies on solution: grown semi-organic thiourea doped l-alanine hydrogenchloride single crystal. Natl. J. Chembiosis **2**(2), 1–5 (2011b)

Malliga, P., Umamaheshwari, R., Joseph-Arul-Pragasam, A.: Studies on the growth aspects of thiourea doped L-alanine hydrogenchloride: a promising NLO Crystal. Adv. Mater. Res. **584**, 70–73 (2012). https://doi.org/10.4028/www.scientific.net/amr.584.70

Malliga, P., Alosious-Gonsago, C., Joseph-Arul-Pragasam, A.: Growth and characterization of Glycyl L-Alanine single crystals for NLO devices. Mater. Sci. **9**(11), 428–432 (2013)

Manimekalai, K., Jayaprakash, P., Padmamalini, N., Rama, S.: The effect of magnesium chloride doping on structural, thermal, optical, nonlinear optical and electrical thermal, optical, nonlinear optical and electrical properties of Potassium Dihydrogen Phosphate single crystal. J Mater Sci: Mater Electron **34**, 171 (2023)

Miller, R.: Optical second harmonic generation in piezoelectric crystals. Appl. Phys. Lett. **5**, 17–19 (1964)

Nijboer, B.R.A., Renne, M.J.: Microscopic derivation of macroscopic Vander waals forces. Chem. Phys. Lett. **2**, 35–38 (1968)

Onitsch, E.M.: Mikroscopia, "Systematic metallographic and mineralogic structures." Mikroscopia **2**, 131–151 (1947)

Pearson, R.G.: Hard and soft acids and bases. J. Am. Chem. Soc. **85**, 3533–3539 (1963)

Penn, D.R.: Wave number dependent dielectrics function of semiconductors. Phys. Rev. **128**, 2093–2097 (1962)

Priyadharshini, E., Vinothkumar, P., Jayaprakash, P., Venda, S.: Crystal growth and physico-chemical characterization of an organic 2-amino-6-methyl pyridinium L-tartrate single crystal for optoelectronic device applications. J Mater Sci: Mater Electron **34**, 1–12 (2023)

Raghavan, C.M., Bhaskaran, A., Sankar, R., Jayavel, R.: Studies on the growth, structural, optical, thermal and electrical properties of nonlinear optical CMTG crystal. Current Appl. Phy. **10**, 479–483 (2010)

Rajarajan, K., Sendil-Kumar, K.: Spectroscopic, optical, thermal and Ac conductivity studies on semiorganic nonlinear optical crystal:AMCTC. J. Therm Anal Calorin **112**, 1297–1302 (2013)

Ramesh, V., Gunasekaran, B., Suresh, P., Sundaravadivel, E., Showrilu, K., Rajarajan, K.: Crystal growth, surface morphology, mechanical and thermal properties of UV-nonlinear optical crystal: Mercury cadmium chloride thiocyanate (MCCTC) single crystal. In OP Conference Series: Materials Science and Engineering, Vol. 872, p. 012175. IOP Publishing (2020)

Ramish, V., Syed, A.S., Jagannathan, K., Rajarajan, K.: Growth, spectroscopic and physicochemical properties of bis mercury ferric chloride tetra thiocynate: A nonlinear optical crystal: MFCTC. Spectochimica Acta Part a: Mole. Biomole. Spectroscopy **108**, 236–243 (2013)

Ravindra, N.M., Srivastava, V.K.: Electronic polarizability as a function of the penn gap in semiconductors. J. Infrared Phys. **20**, 67–69 (1980)

Ravisankar, V., Ramesh, V., Krishnamohan, M., Gunasekaran, B., Sabari-Girisun, T.: IUCrData, "Bis(benzo-15-crown-5-j5O)bariumtetraki(isothiocyanatokN)cobaltate(II). IUCrData **6**, 2414–3146 (2021b)

Ravisankar, V., Ramesh, V., Sridevi, D.V., Gunasekaran, B., Sabari-Girisun, T.C.: Synthesis, growth, structural, physicochemical, linear and nonlinear optical properties of new hybrid [(Ba(C$_{10}$H$_{20}$O$_5$)2. (Mn(SCN)4)] Single crystal. Appl. Phy. A **127**, 1–15 (2021c)

Ravisankar, V., Ramesh, V., Gunasekarana, B., Sabari-Girisun, T.: Synthesis, growth, structural, physicochemical, linear, and nonlinear optical properties of new hybrid [2(C$_{10}$H$_{20}$O$_5$) Ba] [Co (SCN)$_4$] single crystal. J Mater Sci Mater Electron **33**, 9380–9394 (2022)

Ravisankar, V., Ramesh, V., Krishna Mohan, M., Gunasekarana, B., Sabari Girisun, T., Dhanusha, A.: Synthesis, growth, structural and physicochemical properties of a novel linear and nonlinear UV-optical single-crystal for photonic applications: [Ba (C$_{14}$H$_{20}$O$_5$)2.Co (SCN)$_4$]. ECS J. Solid State Sci. Tech. (2021a).

Sakthi, P., Rajasekaran, R., Balasubramanian, D.: Growth, optical, thermal and mechanical behavior of an organometallic nonlinear optical-thiocyanate thiourea potassium chloride (TTPC) Crystal. J. Adv. Phys. **5**, 199–206 (2016)

Saravanan, N., Chidambaram, V., Ravisankar, V.: Growth and characterization of novel semi organic nonlinear optical urea lead acetate single crystal by solution growth technique. J. Mater. Sci: Mater. Electron. **29**, 5009–5013 (2018)

Shanthi, C., Jayapraksh, P., Allen-Moses, S.E., Ravisankar, R.: Physico-chemical properties, SHG and THG studies of an semiorganic NLO material L-glutamic acid nickel chloride. J. Opt. **52**, 347–354 (2023)

Sheik-Bahae, M.S.: Sensitive measurement of optical nonlinearities using a single beam. J. Quantum. Electron. **26**, 760–769 (1990)

Sheldrick, G.M.: SADABS program for area detector absorption correction. University of Gottingen, Germany (1996)

Sheldrick, G.M.: A short history of SHELX. Acta Cryst. **A64**, 112–122 (2008)

Shenbagarajan, P., Jayaprakash, P., Krishnan, S.: Synthesis, crystallization, spectroscopic analysis, NLO, HOMO-LUMO, and LDT of a single crystal of thiourea manganese (II) sulfate. J Mater Sci: Mater Electron **34**, 1–12 (2023)

Shettigar, S., Umesh, G., Chandrasekharan, K., Kalluraya, B.: Third-order nonlinear optical properties and two-photon absorption in newly synthesized phenylsydnone doped polymer. Synth. Met. **157**(15), 142–146 (2007)

Subashini, A., Kumaravel, R., Leela, S., Evans, H.S., Sastikumar, D., Ramamurthi, K.: Synthesis, growth and characterization of 4-bromo-4'chloro benzylidene aniline-a third order nonlinear optical material. Spe Chimica Acta A Mol. Biomole. Spe. **78**, 935–941 (2011)

Van Stryland, E.W., Sheik-Bahae, M., Kuzyk, M.G., Dirk, C.W.: Z-scan Measurements of Characterization Techniques and Tabulations for Organic Nonlinear Materials. Marcel Dekker, Inc, pp. 655–692 (1998).

Vijayabhaskaran, B., Ramachandra-Raja, C.: Influence of metallic substitution on the physical properties of nickel mercury thiocyanate nonlinear optical crystal. Optk **124**, 1366–1368 (2013)

Xu, D., Jiang, M.H., Shao, Z.S.: Study on double base structure model and high frequency doubling crystal of metal organic complex. Synth. Cryst. **16**, 1–7 (1987)